Available online at www.sciencedirect.com
SCIENCE DIRECT®
Journal of Sound and Vibration 286 (2005) 781–798
JOURNAL OF SOUND AND VIBRATION
www.elsevier.com/locate/jsvi

Toward the iterative learning control for belt-driven system using wavelet transformation

Kune-Shiang Tzeng[a,b], Jian-Shiang Chen[a,*]

[a]*Department of Power Mechanical Engineering, National Tsing Hua University, Hsinchu, Taiwan, ROC*
[b]*Department of Electrical Engineering, National United University, Maio-Li, Taiwan, ROC*

Received 4 February 2004; received in revised form 27 June 2004; accepted 25 October 2004
Available online 28 December 2004

Abstract

An iterative learning scheme using wavelet transformation to achieve excellent speed-tracking performance of a belt-driven system is presented in this article. The learning control scheme consists of a proportional feedback controller and a feedforward controller. The learning law updates the control profile from the previous output signal of the feedback controller, which has been processed via the wavelet transformation. Using wavelet transformation, the adverse effect due to unlearnable system dynamics can be drastically attenuated. The convergence of the learning control scheme is thus theoretically guaranteed and the convergent rate can be greatly improved in comparison to other iterative learning schemes. The proposed scheme is applied to the speed tracking for an ink-jet printer and excellent speed-tracking performance is achieved through experimental verification.

1. Introduction

Since Arimoto et al. [1] introduced iterative learning control (ILC), many researchers have been focused on this topic [2,3]. The ILC is a control methodology that improves control system performance over repeated trials. This technique can deal with nonlinear systems, and improve the accuracy of tracking error in applications such as robots that usually involve tasks of

*Corresponding author. Tel.: +886 3 571 5131; fax: +886 3 572 2840.
E-mail address: jschen@pme.nthu.edu.tw (J.-S. Chen).

0022-460X/$ - see front matter © 2004 Elsevier Ltd. All rights reserved.
doi:10.1016/j.jsv.2004.10.014

repetitive nature [4]. Although many sufficient conditions have been available to guarantee the convergence of the learning process, the flexible system does not fit the property of learnable or repeatable. The belt-driven system is a typical system that does not have the learnable property, since the system dynamics does not satisfy the invariance during the iterative process. In most applications, belt-drives are adopted for point-to-point motions, seldom used for speed-tracking tasks, because the belt-flexibility would limit the operational bandwidth of the system during tracking movement. Furthermore, a low-frequency vibration is incurred during normal operation [5] and its amplitude will grow during the iterative learning process. A boundary control methodology for a stretched moving string is proposed by Qu [6]. It applied the ILC to the flexible system whose model is described by a partial differential equation. Cai and Huang [7] proposed the Fourier transformation method in order to reduce tracking error due to the high frequency and repeatable disturbance. For non-repeatable dynamics, zero-phase filtering was used in Refs. [8,9].

In this paper, a novel control methodology applicable to systems with unlearnable dynamics is proposed, so that a belt-driven system can track a pre-specified velocity profile more efficiently through iterative learning. An enhanced iterative learning scheme with wavelet transform is presented, which consists of a feedforward and feedback controller. The iterative learning process employs the current cycle error (CCE) to update the control profile. Using the CCE-type iterative learning process, the convergent rate is more effective than using the previous cycle error (PCE) [10]. For improving the learning behavior, a wavelet transform is employed to filter out the unlearnable dynamics from the feedback control signal before it is used to update the control profile. The wavelet transform is different from the Fourier transform [11]. Fourier transform simply processes the signal information in the frequency domain, so it will lose information in the time domain, while the wavelet transform can decompose a signal into many low-resolution signals, which possess the time and frequency information simultaneously. From the viewpoint of signal processing, the wavelet transform can be designed as a low-pass, high-pass and even a band-pass filter without phase lag [11]. In this paper, following Ref. [8], the convergence analysis is presented. To verify the proposed methodology, a Lexmark Z42 ink-jet printer is employed as the control target and a much-improved speed-tracking performance is achieved in the experimental verification.

2. Problem statement

Although the ILC has been applied in many nonlinear systems and provided satisfactory performance, these systems must satisfy certain restrictions. Among those, the system must be "learnable", this being the most stringent condition. If the system dynamics is invariant and the disturbance is repeatable during the iterative process, the system is called 'learnable'. Unfortunately, most systems such as flexible system or belt-driven system do not satisfy these properties. These motivate the development of the ILC scheme for the system with unlearnable dynamics in practical industrial application. Belt-driven mechanism in motion control is a typical system used to contain unlearnable dynamics. A typical single-axis belt-driven system is shown in Fig. 1(a) where an actuator is adopted to drive a carriage transport via the timing-belt. By using Hamilton's principle, four nonlinear equations and 12 nonlinear boundary conditions were

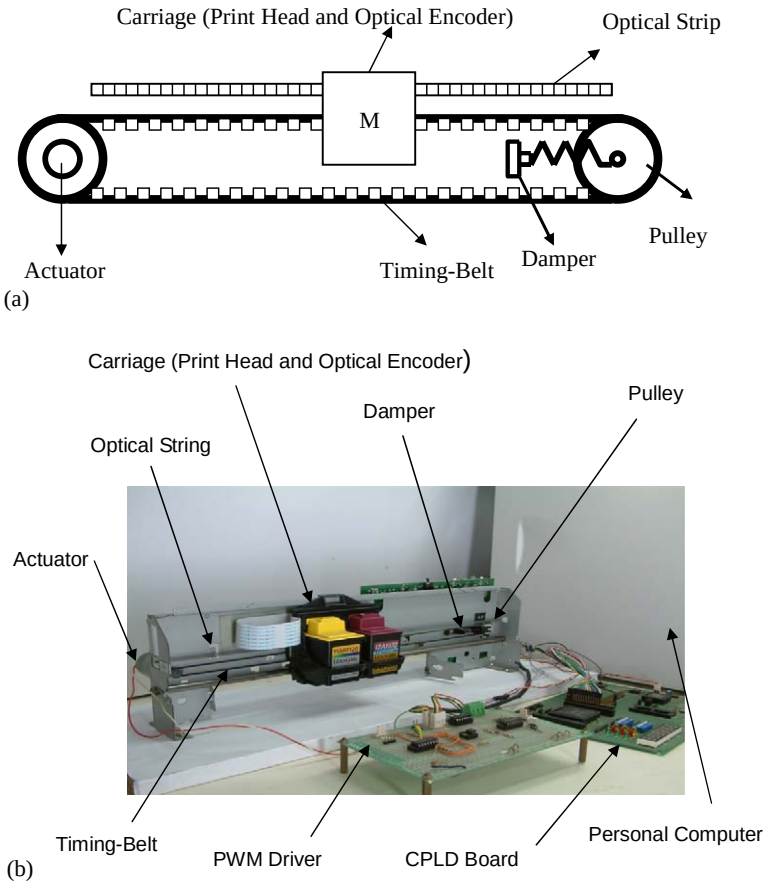

Fig. 1. (a) Mechanical structure of a belt-driven system under study, (b) photo of the belt-driven system under study.

derived for modeling this system [12]. Once the carriage starts to move, not only the overall magnitude of the tension deviates from the one under static conditions but fluctuating components also emerge.

To analyze the dynamics qualitatively, a low-order lumped-parameter model is usually adopted to express the dynamics of the belt-driven system as shown below.

$$m\ddot{x} + F_{\text{ric}}(x, \dot{x}) + d(x) + \vartheta(x, \dot{x}, \ddot{x}) = \tau, \tag{1}$$

where m is the effective inertia of the system, x is the position of the carriage in the fixed reference frame, F_{ric} is the total friction, d is the force due to the load disturbance, ϑ is the force due to the resonant dynamics and τ is the exerted force from the actuator.

In most belt-driven systems, the classical friction model is a combination of Coulomb friction, static friction, viscous friction, and Stribeck effect [13]. As a carriage moves in opposite directions (forward or backward) or under temperature variations due to a long operation, the friction may change differently. The frictional force in the belt-driven systems has previously been modeled [14]

and is herein modified as

$$
\begin{aligned}
F_{\mathrm{ric}}(x,\dot{x}) &= F_f(x,\dot{x}) + F_r(x,\dot{x}),\\
F_f(x,\dot{x}) &= F_{C+}B_+(\dot{x}) + (F_{S+}(x) - F_{C+})\mathrm{e}^{-(v/v_s)^2}B_+(\dot{x}) + \sigma_+(x)v,\\
F_r(x,\dot{x}) &= F_{C-}B_-(\dot{x}) + (F_{S-}(x) - F_{C-})\mathrm{e}^{-(v/v_s)^2}B_-(\dot{x}) + \sigma_-(x)v,
\end{aligned} \tag{2}
$$

where F_{C+} and F_{C-} are the Coulomb coefficients in the forward and backward directions, respectively, and $F_{S+}(x)$, $F_{S-}(x)$ and $\sigma_+(x)$, $\sigma_-(x)$ are the static frictions (including dead-zone) and viscous frictions in the forward and backward directions, respectively. These values on the position of the carriage. Moreover, v_s is the Stribeck velocity; $B_+(\dot{x})$ and $B_-(\dot{x})$ are nonlinear functions having the forms

$$
B_+(\dot{x}) = \begin{cases} 1 & \text{if } \dot{x} > 0,\\ 0 & \text{if } \dot{x} < 0, \end{cases} \quad B_-(\dot{x}) = \begin{cases} 0 & \text{if } \dot{x} > 0,\\ -1 & \text{if } \dot{x} < 0. \end{cases} \tag{3}
$$

Another significant characteristic of elastic elements is the presence of low-frequency oscillatory modes, resulting from transverse and axial belt vibration. The oscillatory amplitude and frequency depend on the initial condition (e.g. carriage position, belt tension, etc.), operating condition (e.g. carriage speed, carriage acceleration, etc.) and boundary conditions (e.g. belt length, limit on exerted force, etc.) that can be synthetically described as follows:

$$
\begin{aligned}
\vartheta(x,\dot{x},\ddot{x}) = {} & \phi_+(x)B_+ \sin(\varpi_+(x,\dot{x},\ddot{x}) + \varphi_+)\\
& + \phi_-(x)B_- \sin(\varpi_-(x,\dot{x},\ddot{x}) + \varphi_-),
\end{aligned} \tag{4}
$$

where $\phi_+(x)$ and $\phi_-(x)$ are the amplitudes at resonance which vary with the position of the carriage. The symbols $\varpi_+(x,\dot{x},\ddot{x})$ and $\varpi_-(x,\dot{x},\ddot{x})$ are the resonant frequencies during forward and backward motion, respectively. $\varphi_+(x)$ and $\varphi_-(x)$ are the angle of time lag between the driving pulley and idle pulley when the belt-driven system is operated. All of these parameters can be determined from experiments, but in practical application they are subjected to change under various operating conditions. At low frequency, a first-order transfer function $G(s)$ can approximate the system dynamics with the output $\dot{x}$ (speed of carriage) and input v_t (armature voltage of motor). From the viewpoint of signal process, the low-frequency vibration due to unlearnable dynamics can be distinguished from the response of the system. In other words, the dynamics of the belt-driven system can be decomposed into a learnable part and an unlearnable part by suitably choosing signal process tools, like the wavelet transform. We then design the ILC scheme to learn learnable dynamics. Thus, the stability would not be destroyed by the unlearnable part. To validate the proposed design, a belt-driven system is constructed as a control target with the new ILC scheme.

3. ILC controller design with wavelet transform

Since the ILC scheme is designed to learn the system dynamics via the repetitive process, the system must satisfy the property of repeatable or learnable. In general, the system dynamics must possess invariant dynamics and the system disturbance must be repeatable during the

iterative process. These properties are difficult to satisfy in flexible systems. Hence, in this paper we propose an iterative learning control using wavelet transformation to overcome this drawback.

3.1. Wavelet transform: a brief review

Wavelets have been applied with success in a wide variety of research areas such as signal analysis, de-noising and image processing [15]. They are particularly suited to the study of transients and that of the local regularity of signals in many practical applications. On the other hand, they are very closely linked to the multi-resolution analysis (MRA). In this paper we adopt the MRA as a new tool for extracting the unlearnable dynamics features in an ILC system and then apply the resultant ILC scheme to the speed tracking of the system with unlearnable dynamics. The MRA is a tool that utilizes the wavelet transform to map a one-dimensional time signal into a two-dimensional signal represented in both the frequency and time domain. The wavelet transform of a time function $f(t)$ with a mother wavelet $\psi(t)$ is defined as the inner product of $f(t)$ with $\psi_{a,b}(t)$, i.e.

$$Wf(a,b) = \langle f(t), \psi_{a,b} \rangle, \tag{5}$$

where a is a scaling factor and b is a shift parameter. The mother wavelet has the form

$$\psi_{a,b} = \frac{1}{\sqrt{a}} \psi\left(\frac{t-b}{a}\right). \tag{6}$$

The mother wavelet $\psi_{a,b}(t)$ is assumed to lie in $L^2(R)$ and satisfies the following conditions:

$$\int_{-\infty}^{+\infty} \psi(t)\,\mathrm{d}t = 0 \quad \text{and} \quad \psi(0) = 0, \tag{C1}$$

$$C_\psi = \int_0^\infty \frac{|\hat{\psi}(\omega)|}{\omega}\,\mathrm{d}\omega < +\infty. \tag{C2}$$

Under conditions (C1) and (C2), $\psi(t)$ can be described as the impulse of a band-pass filter and the wavelet transform may be interpreted as the filtering results through band-pass-filter defined as

$$Wf(a,b) = f^* \psi_a(t) = \frac{1}{a} \int_R f(t) \psi\left(\frac{t-x}{a}\right) \mathrm{d}x. \tag{7}$$

Using the wavelet transformation, the signal $f(t)$ can be decomposed into multiple-level signals. Hence, the signal $f(t)$ is broken down into many lower-resolution components. This process is expressed in terms of the wavelet decomposition tree as shown in Fig. 2. A_n and D_j, $j = 1, 2, \ldots, n$ are called the approximations (low-frequency components) and details (high-frequency components), respectively, and n is the level of decomposition. After the process of decomposition, the original signal $f(t)$ also can be reconstructed through the reconstruction filters as below

$$f(t) = W^* f(t) = A_n + \sum_{j=1}^{n} D_j. \tag{8}$$

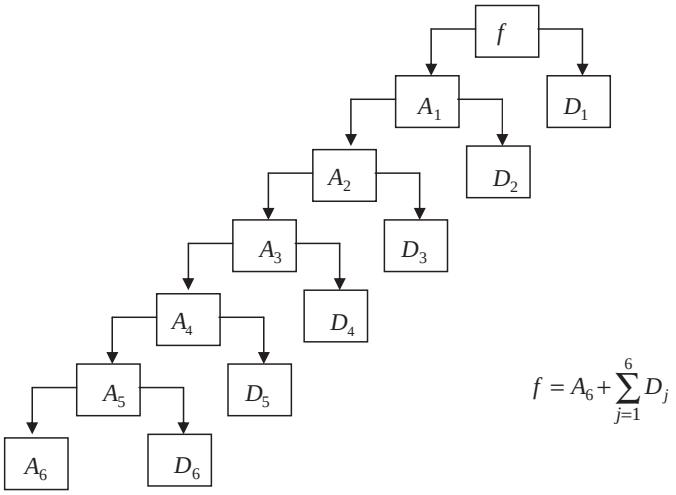

Fig. 2. The wavelet decomposition tree.

In practical applications, some or all of the detail components can be eliminated during the reconstructed process. In other words, the wavelet transform can be a contraction mapping on $f(t)$. To show this fact, let

$$f_1 = W^* f, \tag{9}$$

where the symbol W^* stands for the wavelet transform as a filtering operator. Then we have $\|f_1\|_1 < \|f\|_1$. Denote $\|.\|_1$ as the one-norm of a time function. The following lemma will be useful in the sequel.

Lemma 1. *Suppose that a signal $f(t)$ can be decomposed as Eq. (8) with $A_n > \gamma \sum_{j=1}^{n} D_j$ and $\gamma > 4$. Then there exists a positive real number α, such that wavelet operator $(1 - \alpha W^*)$ is a contraction mapping on $f(t)$, i.e.*

$$\|(1 - \alpha W^*)^k f(t)\|_1 \leqslant \rho^k \|f(t)\|_1 \to 0 \quad \text{as } k \to \infty \text{ for } 0 < \rho < 1.$$

Proof. See Appendix A. □

3.2. An enhanced ILC scheme using wavelet transform

A feedback control system with ILC can always provide good performances on the transient responses and reduce the steady-state error [10] provided that system is learnable. In a flexible system, the ILC controller fails to work properly over the iteration process. In such applications, the ILC controller updates the profile of control effort by using tracking error which is contaminated by low-frequency resonant oscillations; the error will eventually grow up to infinity. In other words, the iterative learning controller will induce system instability due to the unlearnable dynamics inherent in the flexible system. A block diagram of the overall control

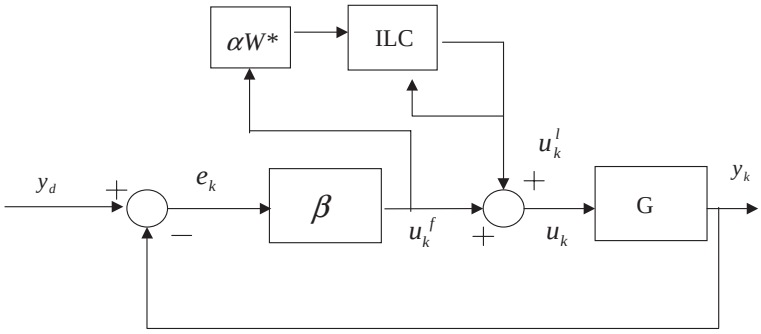

Fig. 3. Block diagram of the proposed control system.

system is shown in Fig. 3, where y_d is the desired output trajectory and y_k is the system output of the kth iteration. The control scheme is expressed as follows:

$$u_k(t) = u_k^l(t) + u_k^f(t), \tag{10}$$

$$u_k^l(t) = u_{k-1}^l(t) + \alpha W^* u_{k-1}^f, \tag{11}$$

$$u_k^f(k) = \beta e_k(t), \tag{12}$$

where α is a positive and fixed learning gain, u_k^f is a proportional feedback controller and u_k^l is the iterative learning controller. The feedback control signal u_k^f is processed by the wavelet transform and then applied to update the learning profile.

In practical applications, it is reasonable to assume that the belt-driven system with transfer function $G(s)$ satisfies the following properties:

(A1) The transfer function $G(s)$ has a positive real part for $0 < w < w_c$, i.e. $\inf_{0<w<w_c} \mathrm{Re}\, G(\mathrm{j}w) > 0$, where w_c denotes the cut-off frequency of the system.

(A2) The control signal $u_k(t)$ can be decomposed into the learnable part $u_d^l(t)$ and the unlearnable part $u_k^{\mathrm{ul}}(t)$, i.e.

$$u_k(t) = u_d^l(t) + u_k^{\mathrm{ul}}(t).$$

(A3) At the kth iteration, the frequency response of the unlearnable part u_k^{ul} is band-pass type and its one-norm is bounded by a small constant after the wavelet transform. That is

$$\| W^* u_k^{\mathrm{ul}} \|_1 \leqslant \varepsilon \quad \forall k.$$

Lemma 2. *Suppose that an ILC system satisfies assumptions* (A1)–(A3) *with the control scheme described as Eqs.* (10)–(12). *Then there exists a real number* $\alpha, 0 < \alpha < 2$ *such that the iterative learning process will converge to a positive small number* $\tilde{\varepsilon}$, *i.e.*

$$\lim_{k\to\infty} \| u_k^l \|_1 \to \| u_d^l \|_1 + \tilde{\varepsilon}.$$

Proof. See Appendix B. □

The unlearnable part of the system response is filtered out by using the wavelet transform. Hence, the learning behavior is improved while the feedback controller improves the transition response due to the unlearnable dynamics or non-repetitive disturbance.

Remark 1. In practical application, the choice of learning gain α and feedback gain β are highly dependent on the frequency response of plant $G(\mathrm{j}w)$. The system cut-off frequency w_c can be utilized to decide these control parameters. The unlearnable dynamics is neglected and $w<w_c$ the system dynamics at the kth iteration can be described as

$$y_k = G(\mathrm{j}w)u_k. \tag{13}$$

Let

$$e_k = y_d - y_k.$$

Applying Eqs. (11)–(13) to Eq. (14), we have

$$e_k = y_d - G(\mathrm{j}w)(u_k^l + u_k^f) = y_d - G(\mathrm{j}w)(u_{k-1}^l + \alpha u_{k-1}^f + \beta e_k). \tag{14}$$

This implies

$$\begin{aligned} e_k(1+\beta G(\mathrm{j}w)) &= y_d - G(\mathrm{j}w)(u_{k-1}^l + u_{k-1}^f + (\alpha-1)u_{k-1}^f) \\ &= y_d - y_{k-1} - (\alpha-1)\beta G(\mathrm{j}w)e_{k-1} \\ &= e_{k-1}[1-(\alpha-1)\beta G(\mathrm{j}w)]. \end{aligned} \tag{15}$$

Thus,

$$\frac{\|e_k\|}{\|e_{k-1}\|} = \frac{\|1-(\alpha-1)\beta G(\mathrm{j}w)\|}{\|1+\beta G(\mathrm{j}w)\|} < 1, \tag{16}$$

for $w<w_c$ and $0<\alpha<2$ $\beta>0$ and $\|.\|$ denoted the two-norm of a time function. Clearly, the convergent rate depends on the values of α and β. When $\alpha = 1$, and according to (A1), the convergent rate becomes

$$\frac{\|e_k\|}{\|e_{k-1}\|} = \frac{1}{\|1+\beta G(\mathrm{j}w)\|} < 1 \quad \text{for } w<w_c. \tag{17}$$

Remark 2. Since the system loop-gain is usually greater than one below cut-off frequency, from Eq. (16), when α is fixed, larger β implies smaller steady-state error at every iteration process and the convergent rate remains unchanged as a small β is adopted. Obviously, using a large β can reduce the initial learning error, but it must be limited in order to ensure that the resonant phenomenon of the flexible system is not excited. We can design the maximum value of feedback gain $\beta_{\max}$ by using the Ziegler–Nichols method [16]. Since β is designed between zero and $\beta_{\max}$ (i.e. $0<\beta<\beta_{\max}$), the overall control signal is equal to the feedback part at the first iteration (i.e. $u_k = u_k^f$ for $k = 1$). According to Lemma 2, when the feedback control signal u_k^f approaches ε and the learning control signal u_k^l approaches u_d^l as $k \to \infty$, the stability of the closed-loop control system is ensured. For a fixed β, the choice of $\alpha = 1$ will achieve a fastest convergent rate as described in Eq. (17).

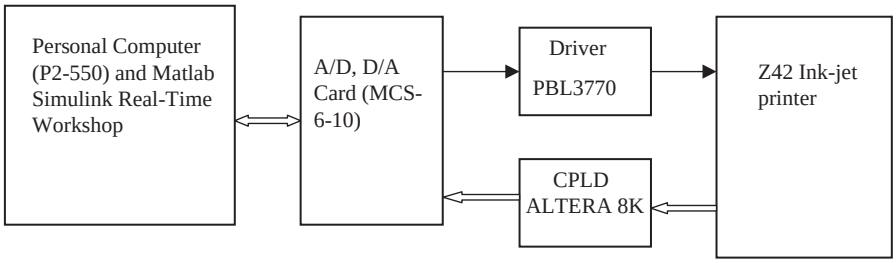

Fig. 4. Schematics diagram of the experimental setup.

4. Experimental results

The configuration of the overall control system is shown in Fig. 4. A DC servo motor equips with an inertia load is the control target. While the DC servo system is utilized for the purpose of speed-tracking control, there exist asymmetrical dead-zones in the forward and backward rotations. Since the shaft of DC motor starts with different angle in every iteration process, this yields different dead-zone for each iteration, which makes a typical non-repeatable system. In other words, the friction can act as a highly nonlinear disturbance on the system. Especially, when the servo system is under heavy load, the friction will vary accordingly. Furthermore, a low frequency vibration will occur due to the variable inertia load. To model the non-repeatable term described above, a general dynamical description of the DC servo system can be expressed as shown in Eqs. (1) and (2). In the hardware setup, a personal computer (P3-550) sends the speed commands to the PWM driver via an A/D card (MCS-6A-C-10), and the shaft position is detected by using a photo encoder delivering two-phase signals (A, B phase). The position data is then fed into to a decoder circuit implemented on a CPLD (Complex Programmable Logic Device) board, which uses an over-sampling scheme [17] to convert the shaft speed into digital format. The controller is realized on the MATLAB, SIMULINK and RTW (Real-Time Workshop) toolboxes.

By using the system identification scheme in the time domain, an experimental transfer function (ETF)

$$G(s) = \frac{188}{s + 28.8} \tag{18}$$

is obtained.

4.1. Determination of a pre-specified speed profile

The pre-specified, $v_d(t)$, is designed to have the following form:

$$v_d(t) = v_{\text{final}} \frac{1}{1 + \mathrm{e}^{-\lambda(t-\gamma)}}, \tag{19}$$

where v_{final} is the final speed of the carriage (in in/s), λ the reciprocal of time constant (ms^{-1}) whose value will be constrained by the bandwidth of the system, i.e. $\lambda < \text{BW}$, once λ is determined,

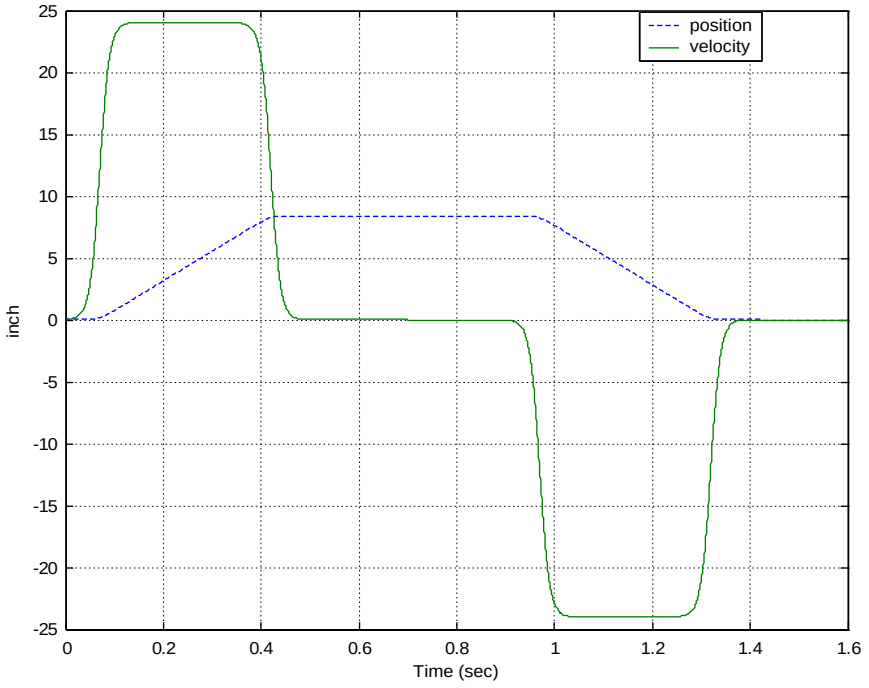

Fig. 5. The desired speed-tracking profile.

and γ can be chosen based on the required distance for acceleration and deceleration. From Eq. (18), the corner frequency of the closed-loop system is around 216.8 rad/s. Thus we can set $\lambda = 200$. Considering the limitation of the power limitation of the actuator, the final speed is selected as $v_{\text{final}} = 24\,\text{in/s}$. Consequently, the value of γ can be chosen based on the distance for acceleration and the acceleration time; if they are less than 1 in and 0.1 s, respectively, then $\gamma = 0.075$. This pre-specified speed profile, $v_d(t)$, is plotted and shown in Fig. 5. It can be seen that both the distance and time for acceleration of the profile, $v_d(t)$, satisfy the requirement.

4.2. Comparison of different ILC schemes

For the purpose of comparison, a CCE-type ILC scheme [19] and a high-order ILC scheme [20] were also implemented. Both schemes utilized the CCE-type that has a more effective convergent rate, rather than using the PCE-type ILC scheme [10]. The algorithms to be implemented are shown as follows.

CCE-type ILC scheme [19]

$$u_{k+1}(t) = u_k(t) + Pe_{k+1}(t), \tag{20}$$

where P is the causal "learning" operator feeding back the current trial error. The physical meaning of this form of learning law is that current trial feedback is obtained causally during the

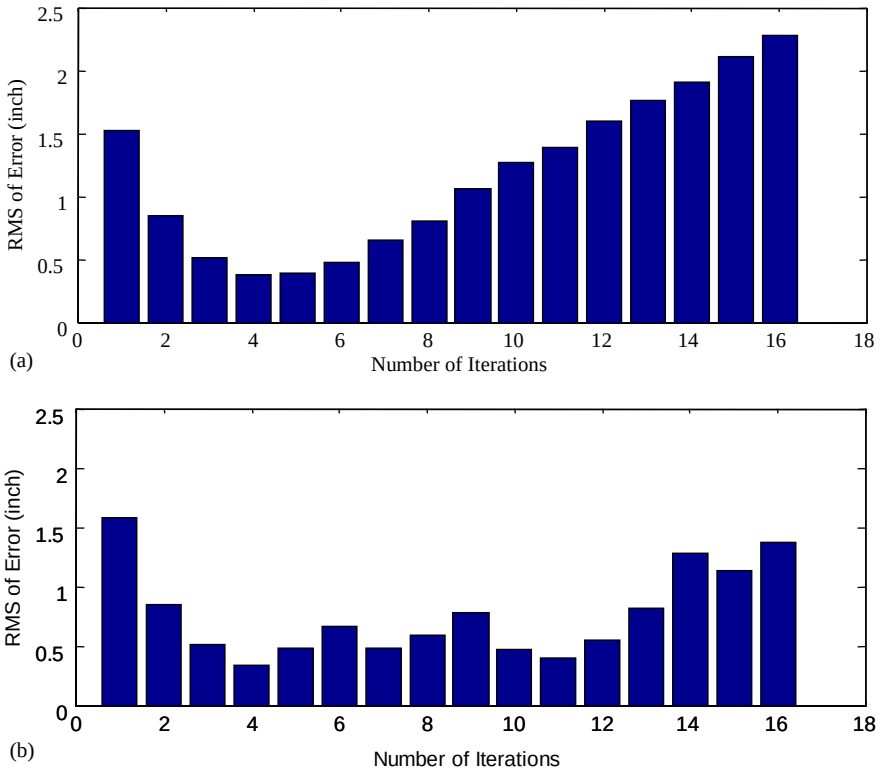

Fig. 6. (a) The learning curve using the simple CCE-type ILC scheme, (b) the learning curve using the high-order ILC scheme.

trial by normal feedback mechanisms for updating the control input [19]. Here, we set $P = 1$ so that the belt-driven system has the maximum feedback gain and will not induce resonance.

High-order P-type ILC scheme [20]

$$u_{k+1}(t) = u_k(t) + \sum_{i=0}^{N} Q_i(t) e_l(t), \tag{21}$$

where $l \equiv k - i + 1; e_l(t) = y_d(t) - y_l(t), N > 0$ and $Q_i(t), i = 0, 1, 2, \ldots, N$ are the learning matrices. For the time-invariant system, the learning gain $Q_i(t)$ can set to be constants. Using the first-order ILC updating law ($N = 1$), the learning gains are chosen as $Q_0 = 0.5$, and $Q_1 = 0.5$. The choice of a suitable Q_i depends on the prior knowledge of the system and the performance index. A detailed description can be found in Ref. [20].

Fig. 6(a) and (b) show the learning curve of both schemes for comparison. Obviously, due to the effect of the low-frequency vibration or the unlearnable dynamics, the learning rates of both schemes tend to diverge after several iterations.

Table 1
The summary of wavelet families and associated properties [15]

Properties	Name							
	Haar	dbN	symN	coifN	mexh	meyr	morl	BiorNr.Nd
Infinitely regular					*	*	*	
Compactly supported orthogonal	*	*	*	*				
Symmetry	*				*	*	*	*
Asymmetry		*						
Near symmetry			*	*				
FIR filters	*	*	*	*				*
Discrete transform	*	*	*	*		*		*
Fast algorithm	*	*	*	*				*
Orthogonal analysis	*	*	*	*		*		
Vanishing moments of ϕ				*				

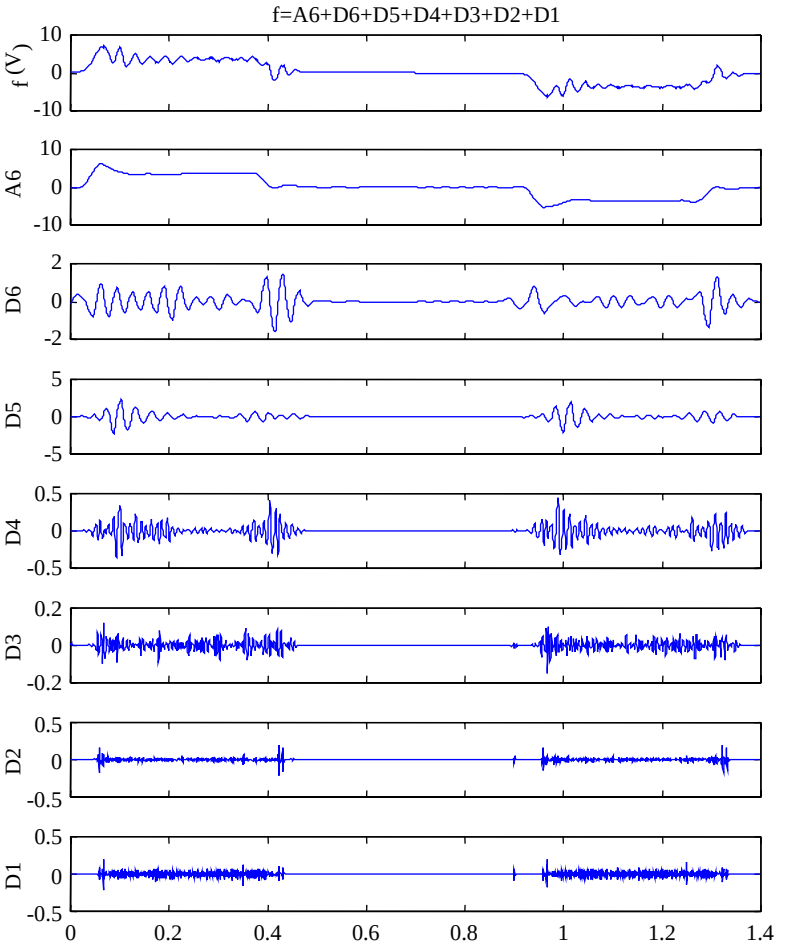

Fig. 7. The wavelet-transformed feedback control signal.

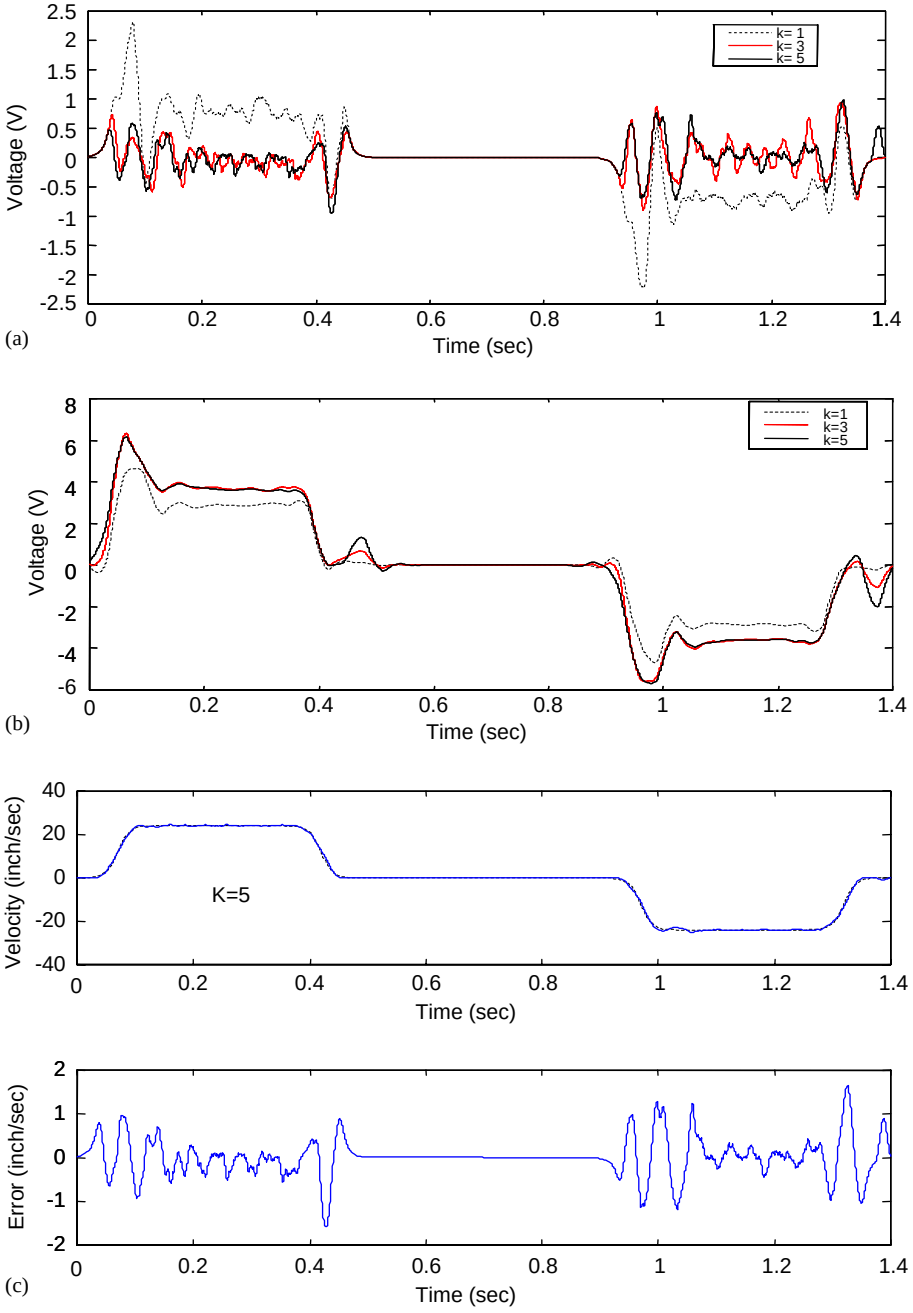

Fig. 8. The control effort and the tracking signal. (a) Feedback term: u_k^f ($\beta = 1$), (b) ILC term: u_k^l ($\alpha = 1$), (c) the speed-tracking profile and tracking error at the fifth iteration. Dotted line: speed command: solid line: carriage speed.

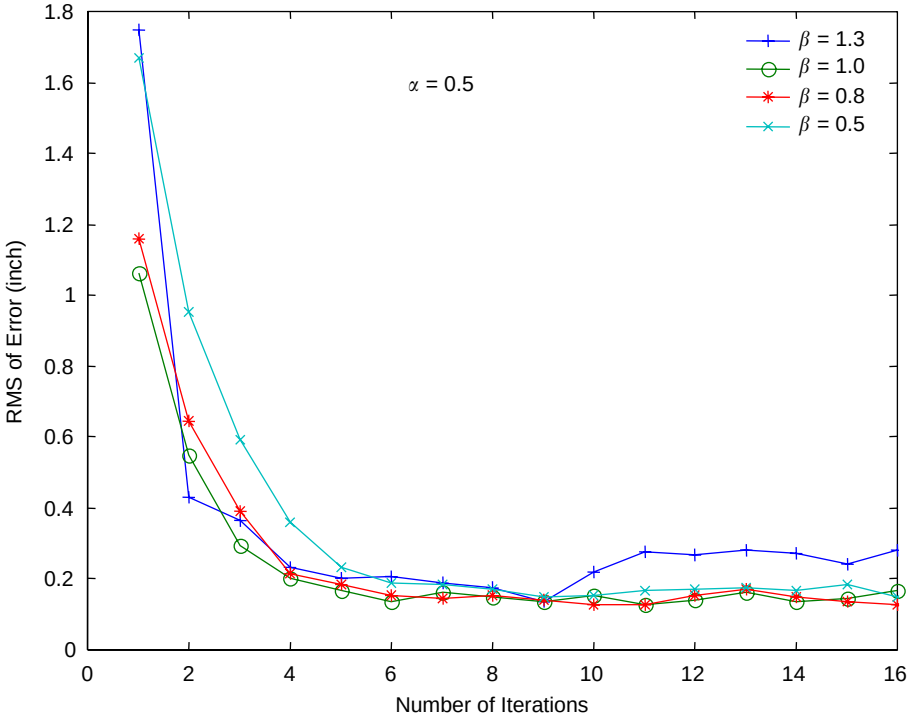

Fig. 9. The learning curve using fixed learning gain ($\alpha = 0.5$) but different feedback gains ($\beta = 0.5-1.3$).

4.3. Experimental verification of the proposed scheme

Step 1 (Selection of wavelet families): Table 1 shows the summary of wavelet families and associated properties [15]. In de-noise processing, it has not been resolved that selecting the appropriate wavelet makes the sequence of wavelet coefficients de-correlate with the original signal. Considering this along with the application of signal process and filter design, we can choose the mother wavelet function which have these features as compactly supported orthogonal, finite impulse response (FIR) and symmetrical or near symmetrical. The SymN were proposed by Daubechies [18] which are modifications from the 'dbN' families, where N is the order. The properties of these two wavelet families are similar. Here, the 'Sym5' function is selected as the mother wavelet and six level details are decomposed.

Step 2 (Selection of learning gain, α, and feedback gain, β): According to the Ziegler–Nichols method [16], when $\beta_{\max} = 1.1$ the resonant phenomenon occurs. The feedback control signal u_k^f is decomposed into six levels as shown in Fig. 7. The signal A_6 is the low-frequency part, corresponding to the learnable dynamics of the belt-driven system and the signals D_1-D_6 are the high-frequency part due to the unlearnable dynamics. The control profiles of feedback and ILC are shown in Fig. 8(a) and (b). After the fifth iteration, the feedback control profile reduces to very small and the ILC profile grows as the A_6 signal that is shown in Fig. 7.

Step 3 (Experimental verification): The speed response and tracking error using the proposed method are shown in Fig. 8 (c), where $\alpha = 1$, $\beta = 1$; this is the case with best convergent rate and

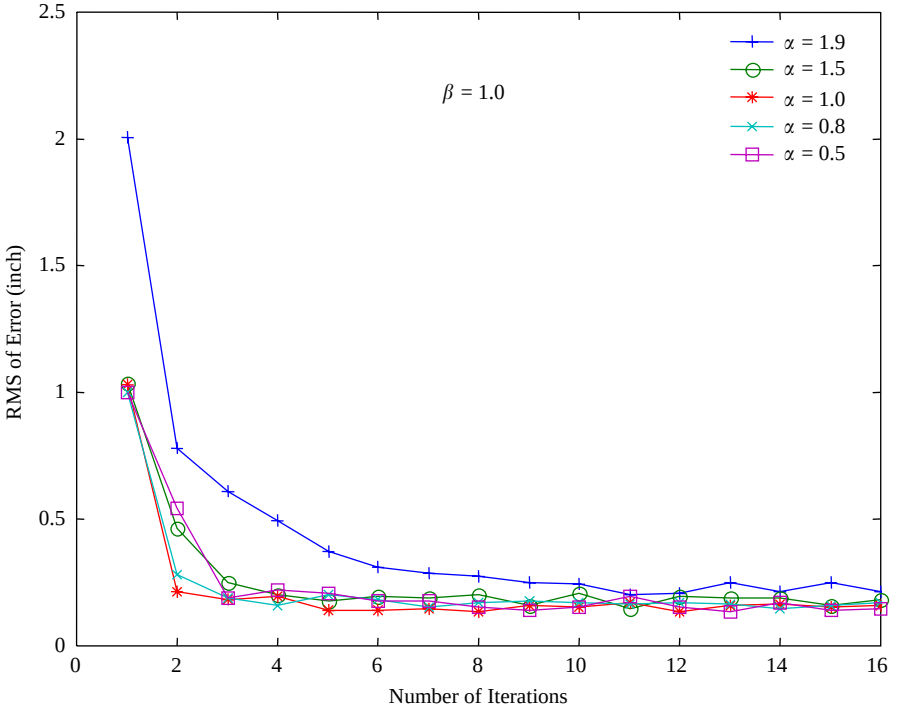

Fig. 10. The learning curve using different learning gains ($\alpha = 0.5-1.9$), but fixed feedback gain ($\beta = 1.0$).

without resonance. To further demonstrate the efficacy of the proposed scheme, Fig. 9 shows the learning curves for fixed learning gain $\alpha = 0.5$ while different feedback gains $\beta = 1.3, 1.0, 0.8, 0.5$ are applied. It is seen that they all exhibit nearly the same convergent rate as anticipated but yield different rms errors at the first iteration due to different closed-loop dynamics. When the feedback gain $\beta = 1.3$, which is larger than $\beta_{\max}$, resonant phenomenon is excited such that the learning curve is unable to converge. Fig. 10 shows the learning curves for the fixed $\beta = 1.0$ but different α, i.e. $\alpha = 0.5, 0.7, 1, 1.5$ and 1.9. They clearly showed that at $\alpha = 1$, it can achieve the best convergent rate as discussed in Remark 2.

5. Conclusions

An iterative learning control scheme using the wavelet transform is proposed and applied to a belt-driven system. The proposed iterative learning scheme is applicable to a belt-driven system with much improved learning behavior. The low-frequency vibration due to the flexibility of belt is significantly reduced during the iterative learning process and the carriage tracks a pre-specified speed profile at high speed with attenuated belt resonant effect. Comparing with other ILC schemes, the proposed method can guarantee the convergence of the learning process even under the influence of unlearnable dynamics. The relation between the learning gain α and the

convergent rate is explicitly exploited and confirmed via experiments. The results further validate the efficacy of the proposed scheme in the ILC system with unlearnable dynamics.

Appendix A. Proof of Lemma 1

From (8), without losses of generality, let $n = 1$. The signal f can be decomposed into

$$f = A_1 + D_1 \tag{A.1}$$

$$\text{with} \quad A_1 > \gamma D_1 \quad \text{for}\, \gamma > 4. \tag{A.2}$$

The detail components can be eliminated during the reconstructed process as described in Eq. (9) such that

$$A_1 = W^* f. \tag{A.3}$$

Then, the following equalities hold:

$$\|f - \alpha W^* f\|_1 = \|(1 - \alpha W^*) f\|_1 = \|A_1 + D_1 - \alpha A_1\|_1 = \|(1 - \alpha) A_1 + D_1\|_1. \tag{A.3'}$$

Applying the property of Eq. (A.2), we obtain

$$\begin{aligned} \|(1-\alpha)A_1 + D_1\|_1 &< \left\| (1-\alpha)A_1 + \frac{A_1}{\gamma} \right\|_1 = \left(|1-\alpha| + \frac{1}{\gamma} \right) \|A_1\|_1 \\ &\leqslant \left(|1-\alpha| + \frac{1}{\gamma} \right) \|A_1\|_1 + \left(|1-\alpha| + \frac{1}{\gamma} \right) \|A_1\|_1 \\ &\quad - 2\left(|1-\alpha| + \frac{1}{\gamma} \right) \|D_1\|_1. \end{aligned} \tag{A.4}$$

Since we can set $0 < \alpha < 2$, and by assumption $\gamma > 4$

$$\left(|1-\alpha| + \frac{1}{\gamma} \right) \|A_1\|_1 - 2\left(|1-\alpha| + \frac{1}{\gamma} \right) \|D_1\|_1 > \left(|1-\alpha| + \frac{1}{\gamma} \right) \|A_1\|_1 - \frac{\rho}{\gamma} \|A_1\|_1, \tag{A.5}$$

where $\rho \equiv 2(|1-\alpha| + 1)/\gamma$.

For $0 < \alpha < 2$, and $\gamma > 4$, we conclude that

$$\rho = \frac{2|1-\alpha| + 2}{\gamma} < 1$$

and

$$|1-\alpha| + \frac{1}{\gamma} - \frac{\rho}{\gamma} = \frac{|1-\alpha|\gamma + 1 - \rho}{\gamma} > 0. \tag{A.6}$$

This implies that

$$\left(|1-\alpha| + \frac{1}{\gamma} \right) \|A_1\|_1 - \frac{\rho}{\gamma} \|A_1\|_1 > 0. \tag{A.7}$$

Hence Eq. (A.4) can be rewritten as

$$\|(1-\alpha)A_1 + D_1\|_1 \leqslant \left(2|1-\alpha| + \frac{2}{\gamma}\right)\|A_1\|_1 - \|D_1\|_1 \leqslant \rho\|A_1 + D_1\|_1, \tag{A.8}$$

where we have used the inequality

$$\|A_1\| - \|D_1\|_1 < \|A_1 + D_1\|_1.$$

Thus,

$$\|(1-\alpha W^*)f\|_1 < \rho\|f\|_1 \Rightarrow \|(1-\alpha W^*)^k f\|_1 < \rho^k\|f\|_1 \to 0 \text{ as } k \to \infty. \qquad \square$$

Appendix B. Proof of Lemma 2

The proof may follow the process described in Ref. [8]. For our case, it is reformulated as follows.

From Eqs. (10) and (A.2), at the kth iteration, the feedback signal is expressed as

$$u_k^f = u_k - u_k^l = u_d^l + u_k^{\mathrm{ul}} - u_k^l. \tag{B.1}$$

Applying the wavelet operator and using (A.3)

$$W^* u_k^f \leqslant W^* u_d^l - W^* u_k^l + \varepsilon. \tag{B.2}$$

Substituting Eq. (B.2) into Eq. (11), it can be obtained

$$u_{k+1}^l \leqslant u_k^l + \alpha(W^* u_d^l - W^* u_k^l + \varepsilon) = (1-\alpha W^*)u_k^l + \alpha(W^* u_d^l + \varepsilon). \tag{B.3}$$

After iterating k in Eq. (B.3), the following inequality holds:

$$u_k^l \leqslant (1-\alpha W^*)^{k+1}u_0^l + [1-(1-\alpha W^*)^{k+1}]u_d^l + \frac{1-(1-\alpha W^*)^{i+1}}{W^*}\varepsilon. \tag{B.4}$$

Since the operator $(1-\alpha W^*)$ is a contraction mapping, $\lim_{k\to\infty}\|1-(\alpha W^*)^{k+1}\|_1 = 0$ as described in Lemma 1.

Eq. (B.4) can be rewritten as

$$\lim_{k\to\infty}\|u_k^l\|_1 \leqslant \|u_d^l\| + \|\tilde{\varepsilon}\|_1, \tag{B.5}$$

where

$$\tilde{\varepsilon} = 1/W^*\varepsilon.$$

While the $\tilde{\varepsilon}$ tends to zero, we get the desired results

$$\lim_{k\to\infty} u_k^l = u_d^l. \qquad \square \tag{B.6}$$

References

[1] S. Arimoto, S. Kawamura, F. Miyazaki, Bettering operation of robots by learning, *Journal of Robotic Systems* 1 (1984) 123–140.
[2] T.J. Jang, C.H. Cho, H.S. Ahn, Iterative learning control in feedback system, *Journal of Automatica* 31 (2) (1995) 243–248.
[3] J.Y. Choi, J.S. Lee, Adaptive iterative learning control of uncertain robotic system, *IEE Proceedings on Control Theory and Applications* 147 (2000) 217–223.
[4] M. Togai, O. Yamano, Analysis and design of an optimal learning control scheme for industrial robots: a discrete system approach, in: *Proceedings of 24th Conference on Decision and Control*, Ft. Lauderdale, FL, 1985, pp. 1393–1398.
[5] M.A. Heckl, I.D. Abrahams, Active control of friction-driven oscillations, *Journal of Sound and Vibration* 193 (1996) 417–426.
[6] Z. Qu, An iterative learning control for boundary control of a stretched moving string, *Automatica* 38 (2002) 821–827.
[7] L. Cai, W. Huang, Fourier base learning control and application to position table, *Robotics and Autonomous Systems* 32 (2000) 89–100.
[8] K.K. Tan, H. Dou, Y. Chen, T.H. Lee, High precision linear motor control via relay-tuning and iterative learning based on zero-phase filtering, *IEEE Transactions on Control System Technology* 9 (2) (2001).
[9] H. Elci, R.W. Longman, M.Q. Phan, J.N. Juang, R. Ugoletti, Simple learning control made practical by zero-phase filtering: applications to robotics, *IEEE Transactions on Circuits and System-I: Fundamental Theory and Applications* 49 (6) (2002).
[10] Z. Bien, J.X. Xu, *Iterative Learning Control, Analysis, Design, Integration and Applications*, Kluwer Academic, Dordrecht, 1998.
[11] A. Cohen, R.D. Ryan, *Wavelets and Multiscale Signal Processing*, Chapman & Hall, London, 1995.
[12] W.T. Rim, K.J. Kim, Identification of tension in a belt-driven system by analyzing flexible vibration, *Journal of Mechanical System and Signal Processing* 8 (2) (1994) 199–213.
[13] B. Armstrong-Helouvry, *Control of Machines with Friction*, Kluwer, Boston, MA, 1991.
[14] W. Li, X. Cheng, Adaptive high-precision control of positioning tables-theory and experiments, *IEEE Transactions on Control System Technology* 2 (3) (1994) 265–270.
[15] Wavelet Toolbox for Use with MATLAB User's Guide, The MathWorks, Inc., 1997.
[16] R.T. Stefani, C.J. Savant, B. Shahian, G.H. Hostetter, *Design of Feedback Control System*, Saunders College, Boston, 1994.
[17] Z.L. Su, A CPLD-Based Servo Controller Design, Master Thesis, Department of Power Mechanical Engineering, National Tsing Hua University, 1998.
[18] I. Daubechies, *Ten Lectures on Wavelets*, SIAM, Philadelphia, PA, 1992.
[19] D.H. Owens, Iterative learning control—convergence using high gain feedback, in: *IEEE Proceedings of the 31th Conference on Decision & Control*, Tucson, AZ, December 1992, pp. 2545–2546.
[20] Y. Chen, C. Wen, M. Sun, A robust high-order P-type iterative learning control using current iteration tracking error, *International Journal of Control* 68 (2) (1997) 331–342.